ON THE NUMERICAL MODELING OF BUOYANCY-DOMINATED TURBULENT DIFFUSION FLAMES BY USING URANS WITH A $k-\varepsilon$ TURBULENCE MODEL

B. Sapa*/, P. Plion**, L. Gay**, F. Nmira**, H. Y. Wang***

wang@ensma.fr

*** Institut P', Fluides, Thermique, Combustion, CNRS, ENSMA, Université de Poitiers, BP 40109 F86961 Futuroscope Chasseneuil Cedex, France**

****EDF R\&D, 6 quai Watier, 78400 Chatou, France**

Abstract

This work concerns the modelling of buoyancy-dominated turbulent diffusion flames through an URANS approach in the Code_Saturne software. It is found that URANS successfully predicts the important features of highly oscillating buoyancy-induced flows (recirculation zone, narrowing and broadening of the flame). Also, the mean velocity, temperature and chemical species are correctly reproduced by URANS. While, the standard $k-\varepsilon$ model should be improved to model the turbulent mixing near the burning wall for a low Froude number flame.

1. Introduction

A large number of studies [1-7] have been performed on the characteristics of buoyant diffusion flames above a horizontal burning surface. Becker et al. [2] have demonstrated that, in the natural convection limit, as the Froude number decreases, coherent structures appear in the reactive zone, the flame presenting a pronounced instability due to buoyancy. Besides, coupling between pyrolysis rate and heat transfer becomes rather complex when fire is confined with severe ventilation condition, where the phenomenon such as extinction and reinflamation or ghost flames appear. Thus, a low Froude number flame in free conditions has already been largely studied [3-7] by using a porous burner. The detailed measurements of the flame and flow structures have been obtained with medium-scale fires [4]. For a low Froude number flame, shear-stresses between hot combustion products and fresh air make the flow unstable and amplify oscillations near the fire base (Weckman [6]) due to air entrainment variation and flame flicker, inducing large eddy structures corresponding to hot gases puffs burning. Fresh air entrained by these vortexes feeds the flame with oxygen and cools the smoke influencing natural convection and then air entrainment. Computational Fluid Dynamics are expected to improve understanding and prediction, by its local description of such buoyancy-controlled flow, of the gas composition and thermal exchanges. Several authors [7] have shown the limit of the use of Reynolds Averaged Navier-Stokes (RANS) $k-\varepsilon$ turbulence model to simulate the highly oscillating buoyancy-induced flow. In order to capture the buoyancy-controlled flow at industrial scale, Large Eddy Simulation (LES) and Unsteady Reynolds Average Navier-Stokes (URANS) method are currently employed. The accuracy of LES depends on filtering scale related to mesh size, and a few millions cells is usually needed for a good description of combustion scales. URANS method is based on

Reynolds average equations and the definition of ensemble (or time, under ergodic hypothesis) averaging implies that scales smaller than a characteristic time are modelled and the other are solved through mean flow. The solution is assumed to be an averaged one in which turbulent effects are considered through turbulence models. In general, URANS allows less refined meshes than LES can do and time calculation becomes reasonable for cells width adapted to the modelling. With this main motivation, EDF R&D has developed an URANS approach in a CFD freeware Code_Saturne [8] for industry application such as gas turbines, coal furnaces, compressible flows, gas-particles interactions or electric arcs. It is found that a fluctuating, laminar, diffusion flame at the fire base, and a turbulent, intermittent one as it evolves upward along the fire plume are better described by URANS approach. The mean temperature, velocity and main chemical species, provided from URANS, are also compared with the experimental data, and a good agreement is observed.

2. Physical Modelling

The simulations were performed using the Code_Saturne software [8], in which combustion is modelled by a turbulent diffusion flame model using a presumed probability density function. Chemistry is described by an infinitely fast global reaction at a constant stœchiometric ratio. The starting point of the analysis is the set of three-dimensional elliptic, reacting flow equations that governs the phenomena of interest here. This set consists of the conservation equations of mass, momentum, energy and species. Density is calculated by the perfect gas law. Two equations are solved for turbulent kinetic energy k and its dissipation rate ε [9]. A finite volume technique is used to discretize the partial differential equations. The precise formulation of the differential equations describing the model and the numerical technique can be found elsewhere [8], and will not be repeated here. In the following section, only URANS approach and radiation associated with soot formation, developed by the authors in Code_Saturne, are briefly described.

2.1 Unsteady RANS approach

URANS is based on a Favre meaning operation which decomposes a full flow field Φ (x, t) into a mean component $\overline{\Phi}$ (x, t) (ensemble average) and a fluctuation Φ''(x, t). Meaning the exact equations of mass and momentum, averaged equations are obtained:

$$\frac{d\overline{\rho}}{dt} + \overline{\rho}\,\mathrm{div}\,\underline{\widetilde{u}} = \Gamma \tag{1}$$

$$\frac{d\overline{\rho}\underline{\widetilde{u}}}{dt} + \mathrm{div}\left(\overline{\rho}\underline{\widetilde{u}}.\underline{\widetilde{u}}\right) = -\,\underline{\mathrm{grad}}\,\overline{p} + \mathrm{div}\,\underline{\underline{\widetilde{\tau}}} + S_u \tag{2}$$

In Code_Saturne, thermal expansion is not taken into account in SIMPLEC algorithm for Navier-Stokes system resolution due to neglecting the mass accumulation term in continuity equation. The new procedure, named as URANS, accounts for the thermal expansion in continuity equation through density-velocity coupling resolution. Based on a low Mach algorithm, this approach is developed still from a two-step scheme with a prediction step which considers momentum equation treated with an explicit pressure and uses mass equation for density derivative versus time.

$$\overline{\rho}\frac{d\underline{\widetilde{u}}}{dt} + \underline{\widetilde{u}}\left[\Gamma - \mathrm{div}(\overline{\rho}\underline{\widetilde{u}})\right] + \mathrm{div}\left(\overline{\rho}\underline{\widetilde{u}}.\underline{\widetilde{u}}\right) = -\,\underline{\mathrm{grad}}\,\overline{p} + \mathrm{div}\,\underline{\underline{\widetilde{\tau}}} + S_u \tag{3}$$

It gives a predicted velocity $\underline{u}^*$, and a correction step which considers mass equation (1) and time-discretizised momentum correction equation ($\delta p^{n+1} = p^{n+1} - p^n$):

$$\bar{\rho}\frac{d\tilde{\underline{u}}}{dt} = -\underline{\text{grad}}\,\delta\bar{p}^{n+1} \Rightarrow \tilde{\underline{u}}^{n+1} - \underline{u}^{*} = -\frac{\Delta t}{\bar{\rho}}\underline{\text{grad}}\,\delta\bar{p}^{n+1} \tag{4}$$

Replacing corrected velocity in divergence of equation (4) by adequate form of equation (1), an equation for pressure increment is obtained:

$$\text{div}\left(-\frac{\Delta t}{\bar{\rho}}\underline{\text{grad}}\,\delta\bar{p}^{n+1}\right) = \text{div}\,\tilde{\underline{u}}^{n+1} - \text{div}\,\underline{u}^{*} = \frac{1}{\bar{\rho}}\Gamma - \frac{1}{\bar{\rho}}\frac{d\bar{\rho}}{dt} - \text{div}\,\underline{u}^{*} \tag{5}$$

For a density dependant of one scalar $\rho(\phi)$, from non-conservative forms of mass and scalar equation:

$$\frac{d\bar{\rho}}{dt} + \bar{\rho}\,\text{div}\,\tilde{\underline{u}} = \Gamma \tag{6}$$

$$\bar{\rho}\frac{d\tilde{\phi}}{dt} = \text{div}\left(\bar{\rho}D\,\underline{\text{grad}}\,\tilde{\phi}\right) + \bar{\rho}S_{\tilde{\phi}} \tag{7}$$

By multiplying Eq.(6) and making density particular derivative appearing in Eq.(7), the velocity divergence can be expressed as:

$$\text{div}\,\tilde{\underline{u}} = \frac{1}{\bar{\rho}}\Gamma - \frac{1}{\bar{\rho}^2}\frac{\partial\bar{\rho}}{\partial\tilde{\phi}}\left[\text{div}\left(\bar{\rho}D\,\underline{\text{grad}}\,\tilde{\phi}\right) + \bar{\rho}S_{\tilde{\phi}}\right] \tag{8}$$

and is used in correction step of Navier-Stokes resolution :

$$\text{div}\left(-\frac{\Delta t}{\bar{\rho}}\underline{\text{grad}}\,\delta\bar{p}^{n+1}\right) = \frac{1}{\bar{\rho}}\Gamma - \frac{1}{\bar{\rho}^2}\frac{\partial\bar{\rho}}{\partial\tilde{\phi}}\left[\text{div}\left(\bar{\rho}D\,\underline{\text{grad}}\,\tilde{\phi}\right) + \bar{\rho}S_{\tilde{\phi}}\right] - \text{div}\,\underline{u}^{*} \tag{9}$$

Corrected velocity is deduced from predicted one and pressure increment through:

$$\tilde{\underline{u}}^{n+1} - \underline{u}^{*} = -\frac{\Delta t}{\bar{\rho}}\underline{\text{grad}}\,\delta\bar{p}^{n+1} \tag{10}$$

2.2 Radiative heat transfer

In a heavily sooting flame as fire, as the radiation spectrum of soot is continuous, it is possible to assume that the gas behaves as a gray medium. The spectral dependence is then lumped into one absorption coefficient, κ, and the following radiative transfer equation without scattering is solved.

$$\vec{\nabla}.\vec{\Omega}I + \kappa I = \kappa\frac{\sigma\tilde{T}^4}{\pi} \tag{11}$$

The overall absorption coefficient is calculated from a grey gas Modak's regression [10] in function of the temperature and the mixture concentration of soot and gas (CO_2 and H_2O). For this, the soot formation and its oxidation are incorporated into a turbulent flow calculation in two convection-diffusion equations for the soot number density, n, and soot volume fraction, f_v, expressed as follows,

$$\frac{\partial\rho\tilde{n}}{\partial t} + \frac{\partial(\rho\tilde{u}_i\tilde{n})}{\partial x_j} - \frac{\partial}{\partial x_j}\left(\frac{\mu_t}{Sc_t}\frac{\partial\tilde{n}}{\partial x_j}\right) = \dot{\omega}_n \tag{12}$$

$$\frac{\partial\rho\tilde{f}_v}{\partial t} + \frac{\partial(\rho\tilde{u}_i\tilde{f}_v)}{\partial x_j} - \frac{\partial}{\partial x_j}\left(\frac{\mu_t}{Sc_t}\frac{\partial\tilde{f}_v}{\partial x_j}\right) = \dot{\omega}_{fv} \tag{13}$$

The local formation rate, $\dot{\omega}_n$, for the soot number density, and $\dot{\omega}_{fv}$, for the soot volume fraction is calculated as,

$$\dot{\omega}_n = C_\alpha N_0 \rho^2 \tilde{T}^{1/2} \tilde{X}_F e^{-T_\alpha/\tilde{T}} - \frac{C_\beta}{N_0} \tilde{T}^{1/2} \tilde{n}^2 - \frac{(36\pi)^{1/3} W_{ox} \tilde{n}^{4/3}}{\rho_{soot} \tilde{f}_v^{1/3}} \quad (14)$$

$$\dot{\omega}_{fv} = \frac{C_\delta}{\rho_{soot}} C_\alpha \rho^2 \tilde{T}^{1/2} \tilde{X}_F e^{-T_\alpha/\tilde{T}} + \frac{C_\gamma}{\rho_{soot}^{1/3}} \rho \tilde{T}^{1/2} \tilde{X}_F e^{-T_\gamma/\tilde{T}} \tilde{n}^{1/3} \tilde{f}_v^{2/3} - \frac{(36\pi)^{1/3} W_{ox} \tilde{n}^{1/3} \tilde{f}_v^{2/3}}{\rho_{soot}} \quad (15)$$

where N_0 (6.022 10^{26} /kmol) is the Avogadro's number, and ρ_{soot}, the soot density, given as 1800 kg/m^3. The empirical constants, such as $C_\alpha(6.54\times10^4$ m^3.kg^{-2}.K$^{-1/2}$.s^{-1}), $C_\beta(1.3\times10^7$ m^3.K$^{1/2}$.s^{-1}), C_δ(144 kg), C_γ(0.1 m^3.kg$^{-2/3}$.K$^{-1/2}$.s^{-1}), $T_\alpha(4.6\times10^4$ K) and $T_\gamma(1.26\times10^4$ K) were experimentally determined by Moss et al. [11] for a range of fuel. The first term in Eq.(14) represents the rate of particle nucleation and the second the coagulation of soot. The second term in Eq.(15) represents the surface growth of soot which contained a linear dependence on aerosol surface area. The term, ω_{ox} (kg/m^{2}s), on the right hand side of Eqs.(14-15) corresponds to soot oxidation which is evaluated from the rate for oxidation of pyrolitic graphite by O_2 [12].

3. Results and discussion

The propane diffusion flames are chosen for comparison between predictions and experiments by using URANS with a turbulence model, $k-\varepsilon$. The free boundaries are located sufficiently far away from the fire to minimize a numerical perturbation. The 3D computational domain are 2.4 m x 2.4 m x 1.5 m in the x, y and z directions, respectively.

Here we concentrate on a comparison of the simulation predictions with the experimental data [4] for a pool diameter, D, of 0.3 m. The flame is stabilized on a horizontal circular porous burner, providing a heat release rate (HRR) in a range from 16, 23 to 38 kW. Temperatures were obtained by thermocouples and velocities were determined using a two-component laser Doppler velocimetry (LDV) system. Only the experimental data in the symmetrical plane is available, and the numerical results are examined in the plane, x-z.

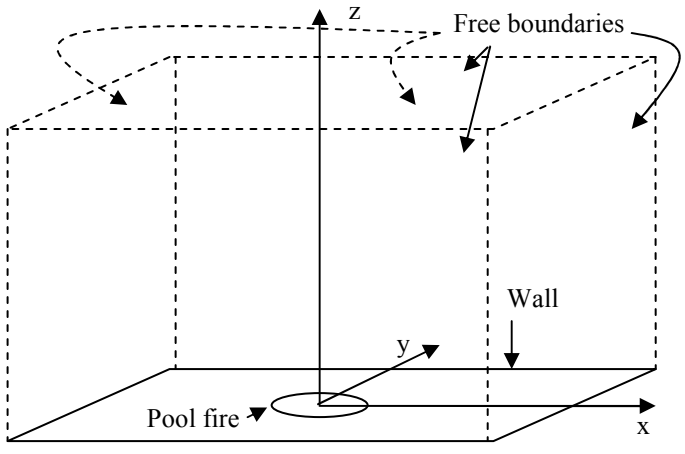

Figure 1. Schematic diagram of the release examined experimentally including the free boundary and the coordinate system.

In order to have a true predictive capability, grid refinement studies were performed, by using a series (Mesh 1-4) of a typical 3D grid points containing, 24(x) x 24(y) x 28(z), 30(x) x 30(y) x 35(z), 90(x) x 90(y) x 60(z) and 130(x) x 130(y) x 90(z) cells, respectively. For a fire plume, the characteristic length scale can be estimated from a given HRR [13], and the HRR considered here is higher than 20 kW, thus the characteristic length is in an order of 0.1 m. The extra grid points are added in the fire region where a strongly stratified layer is developed. At the fire source base, the length scale, Δ, is of the order of 3, 2, 1 to 0.5 cm by using the four grid systems (Mesh 1-4), respectively. Cell sizes are uniform near the fire

source and stretch to about 5 cm far away from the pool-fire region at the free boundary. About 3 days CPU time are needed for a real 1 minute simulation on a 42 processors. Influence of number of grid cells on the predicted temperature and velocity is checked in Figures 2 and 3 for a heat release rate of 23 kW. The changes between the coarse Mesh 1 and fine Mesh 3 in the calculated plots of temperature and velocity above the fire source base are higher than 60%. A further reduction in the grid size (Mesh 4) results in a significant reduction in the time step ($\Delta t \approx 0.001$ s) for satisfying the CFL stability condition. An adequate resolution of the fire plume in large-scale can be achieved with a spatial resolution of about 0.01 m. Finally, the Mesh 3 with 90(x) x 90(y) x 60(z), are employed because it gives the best trade-off between accuracy and cost for the present purpose.

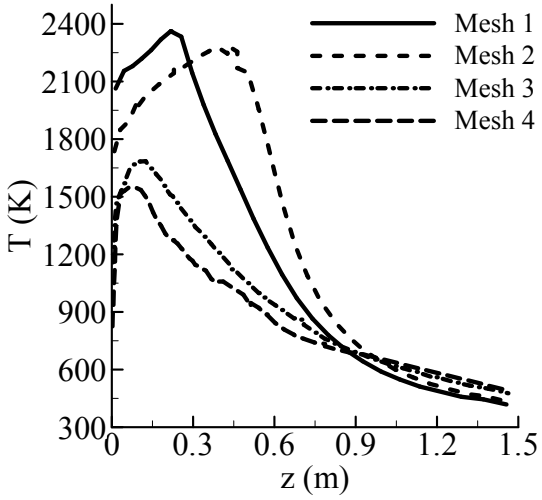

Figure 2. Influence of number of grid cells on the predicted temperature

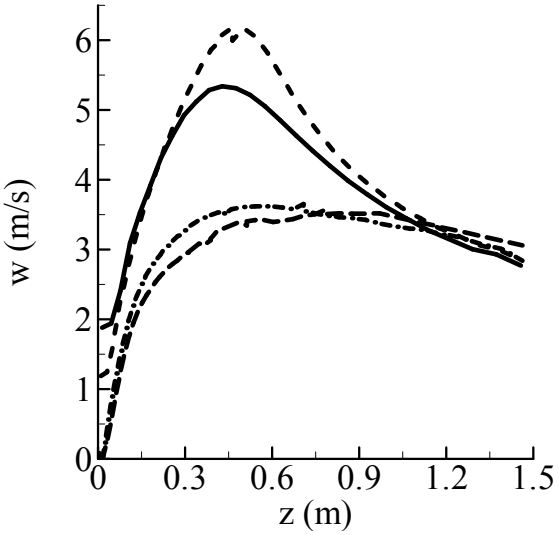

Figure 3. Influence of number of grid cells on the predicted vertical velocity

Based on the grid system Mesh 3, effects of soot formation and gas radiation on the mean temperature T, are shown in Fig.4, as compared with the experimental data. It can be seen that in the plume zone, the temperature peak decrease progressively by accounting for the radiation and soot formation. The calculated maximum values are in good agreement with experiments, while the position of the flame is far away the measured one. The use of the URANS coupled with one-step irreversible chemical reaction is not sufficient to improve the prediction of the flame structure, and the lateral spread of the diffusion flame is usually under-predicted.

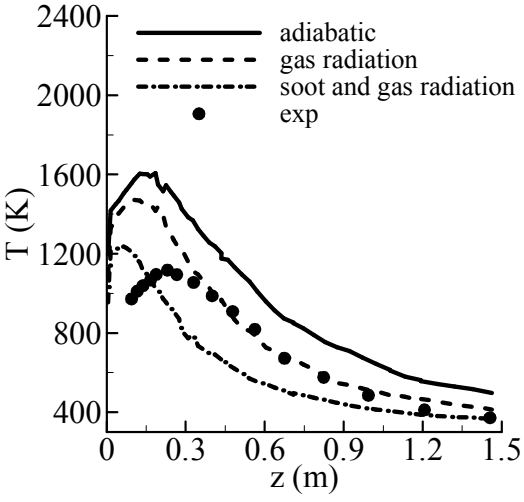

Figure 4. Effects of soot formation and gas radiation on the mean temperature

The calculated characteristics of the instantaneous temperature output on the middle plane (x-z, y=1.2 m) is plotted in Figs.5 and 6 by using RANS and URANS, respectively. The RANS approach generates a stable diffusion flame, and the flow behaves as a boundary layer

type. While three regions of the pool fires are reproduced by URANS approach. At the flame base, immediately above the burner surface, is the persistent flame zone, which appears to have a constant shape and structure. This zone is followed by the intermittent zone that has a fluctuating character due to buoyant instability. In this region, ambient air is sucked into the flame from a downstream location, creating a large recirculating zone above the horizontal burner. The last region is the plume zone that is non reacting and turbulent, giving a good idea of the flow development and the boundary layer broadening. In general, the large scale structure can be completely described when the characteristic length is spanned by roughly ten computational cells. The greater temporal and spatial fidelity can be considered to be extracted by using URANS with Mesh 3 for an application to three-dimensional pool-like fire.

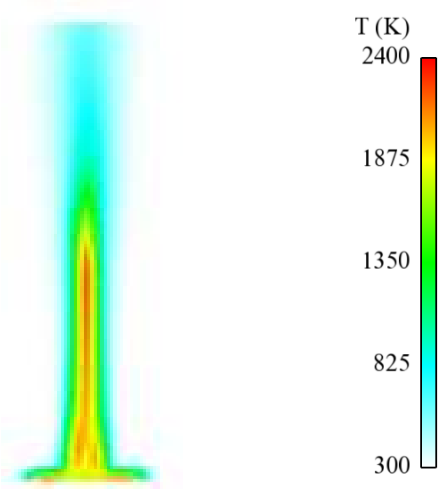

Figures 5. Instantaneous temperature output from RANS

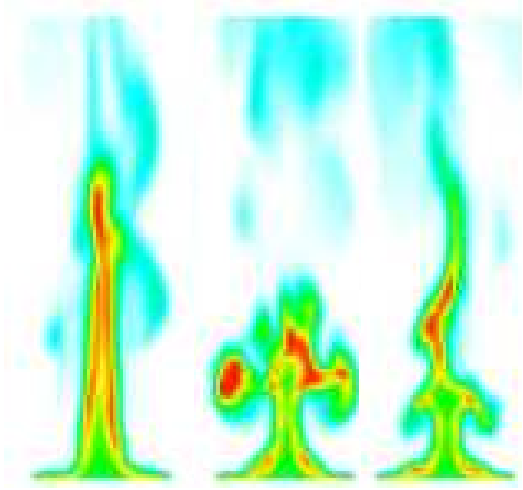

Figures 6. Instantaneous temperature output from URANS

URANS approach can provide a detailed description of the oscillatory behaviour for the buoyancy-driven fire. Determination of the oscillatory behaviour is also important for the spread of fire and hot gases. The simulated time histories of the temperature in the combusting portions of the plume at z = 0.3 m, for a heat release of 23 kW are depicted in Figure 7. The time traces indicate that a large oscillatory fluctuation in the temperature is captured by the time-resolved calculations. This behaviour could manifest itself as the puffs of the plume, and the amplitude of the oscillation of the temperature is as large as about 500°C. The spectral analysis (cf. Fig.8) from prediction suggest that the buoyancy-driven flow produces oscillatory behaviour in cyclic fashion, with a frequency between 2 and 3 Hz, which is commonly observed in experiments and agrees with Zukoski's correlation [5].

Even if the grid size in Mesh 3 is sufficiently small, an incompressible approach (RANS) or a compressible one (URANS) influences significantly the profiles of the mean temperature, T, and the longitudinal velocity, w, along the axial distance, as compared with the experimental data in Figs.9 and 10. Profiles of the longitudinal velocity fluctuation, w", and the transversal one, u", obtained from the two approaches RANS and URANS are also compared with the experimental data in Figs.11 and 12. The velocity fluctuation predicted by the RANS is unrealistically low at the fire base, indicating that this approach can not reproduce the expanded zone of hot gases which coincides with the periodic formation of large coherent structures (cf. Fig.6). The significant over-prediction of the mean temperature and velocity (cf. Figs.9 and 10) with RANS is certainly due to underestimation of the resolved buoyant instability. Subsequently, the flame behaves as a laminar type, causing a higher flame

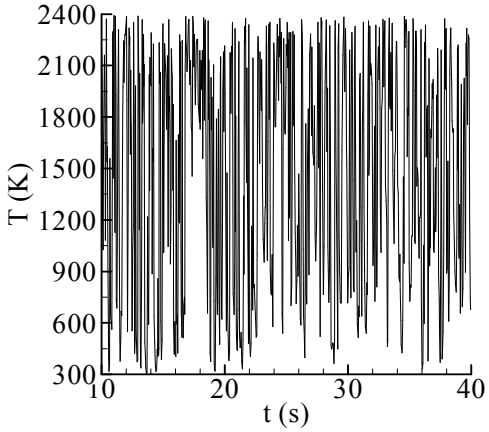

Figure 7. Time traces of a large oscillatory fluctuation in the temperature

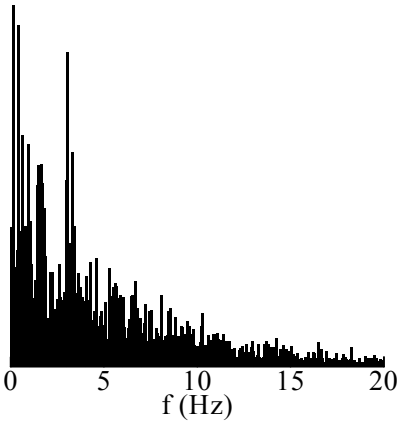

Figure 8. Spectral evolution of the oscillatory behaviour in the temperature

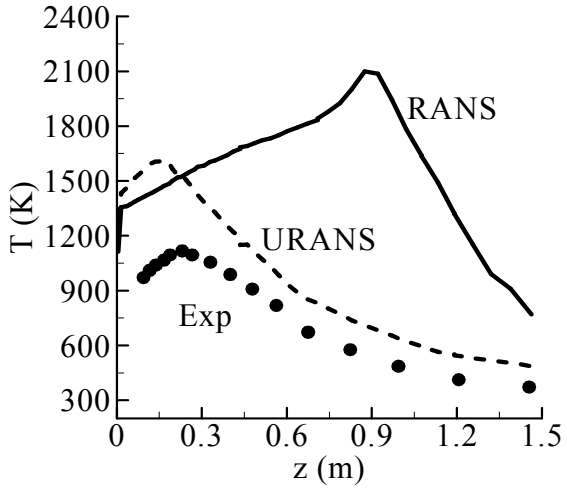

Figure 9. Comparison between the measured and predicted mean temperature from RANS and URANS

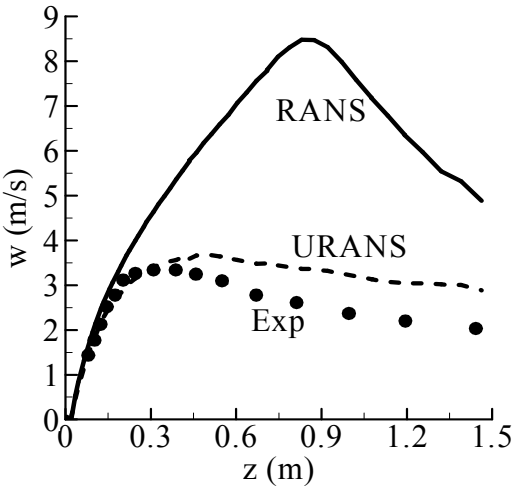

Figure 10. Comparison between the measured and predicted mean longitudinal velocity from RANS and URANS

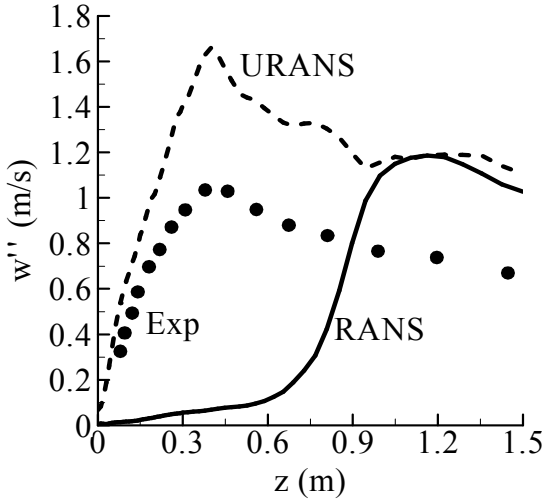

Figure 11. Comparison between the measured and predicted longitudinal velocity fluctuation from RANS and URANS

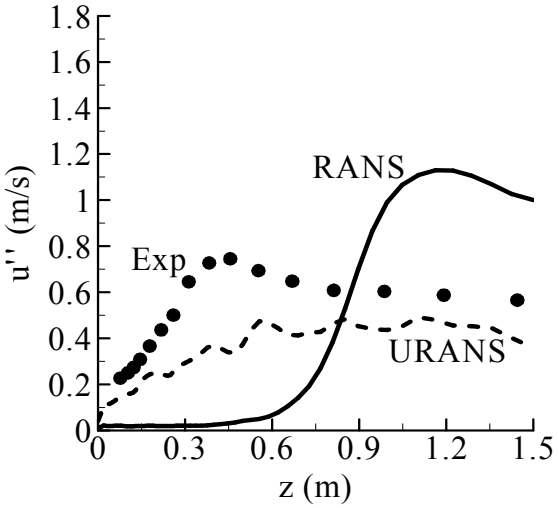

Figure 12. Comparison between the measured and predicted mean transversal velocity fluctuation from RANS and URANS

temperature as compared to the experiment. At the fire region, the underprediction of u" and w" highlights the serious shortcoming in the RANS approach [7] which fails to model the turbulent mixing there even with a fine Mesh 3. For the buoyancy-controlled fire, the oscillation of the flame from buoyant instability is initially taking place near the edge of the horizontal burner surface, where turbulence is weak due to a low fuel injection velocity. The high levels of the velocity fluctuation (u'' and w'') due to the presence of large-scale coherent structures are correctly predicted by URANS.

The profiles of the mean temperature, T and the longitudinal velocity along the axial distance for the HRRs of 16 and 38 kW are also compared with the experimental data in Figs.13-16. In general terms, the comparison between URANS prediction and experiment is reasonably good, although the longitudinal velocity is clearly underestimated. Globally, the approach of URANS is capable of reproducing the mechanism generating the buoyant instability present in the early development of the flame and the transition to turbulence far away from the fire source (z < 0.5 m).

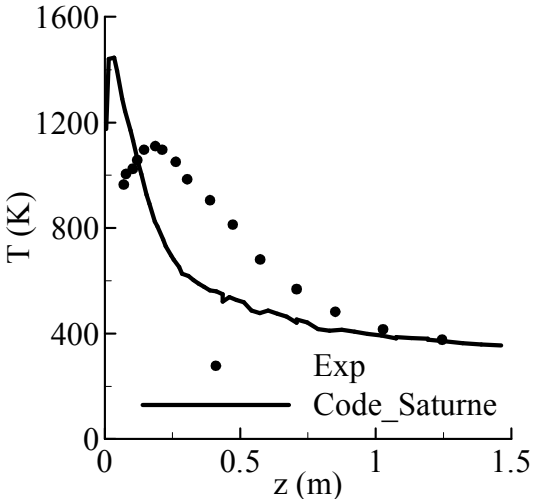

Figure 13. Comparison between the measured and predicted mean temperature for HRR of 16 kW

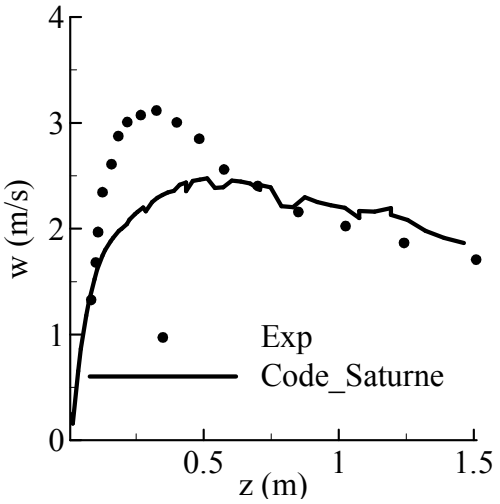

Figure 14. Comparison between the measured and predicted vertical velocity for HRR of 16 kW

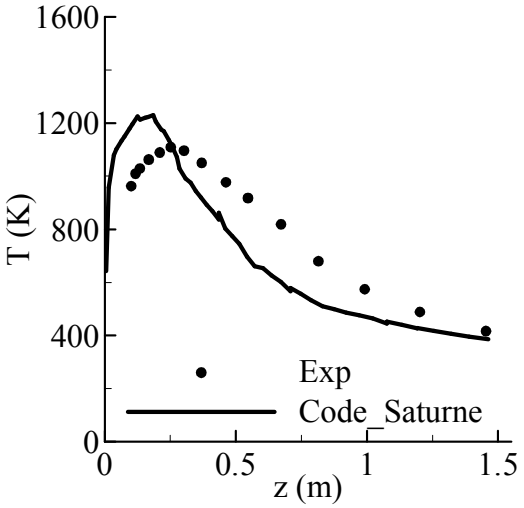

Figure 15. Comparison between the measured and predicted mean temperature for HRR of 38 kW

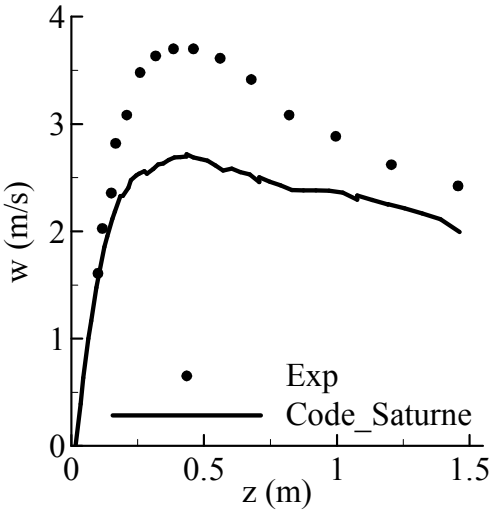

Figure 16. Comparison between the measured and predicted vertical velocity for HRR of 38 kW

Figures 17-22 show the profiles for the mean mass fraction of the chemical species C_3H_8, CO_2 and O_2 along the axial distance. The experimental data show that just above the burning wall, a fuel-rich zone develops and sharply disappears as we move away from the pool fire surface. A strong mixing between the fuel vapour and air probably results from a convective type of mixing rather than from a diffusive one, which gives to the reaction zone a premixed rather than diffusive character. Evident in Figs.17, 19 and 21 is the good agreement between the predicted and the measured values of O_2. As shown in Fig.21, the quality of the agreement between the URANS prediction and experiment for fuel mass fraction deteriorates with an increase of the HRR. The URANS simulation suggests that the reacting flowfield is displaced in a stronger flapping manner. As we move away from the burning surface, the fuel and CO_2 concentrations seem significantly over-predicted. This divergence between prediction and experiment is certainly due to the standard $k-\varepsilon$ model which fails to model correctly the turbulent mixing near the reacting region.

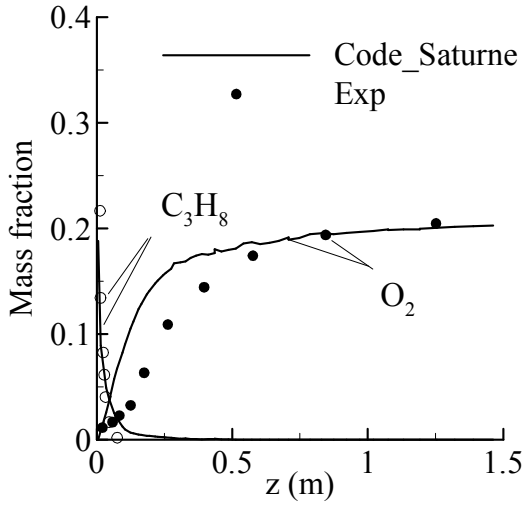

Figure 17. Comparison between the measured and predicted mean fuel and oxygen concentrations for HRR of 16 kW

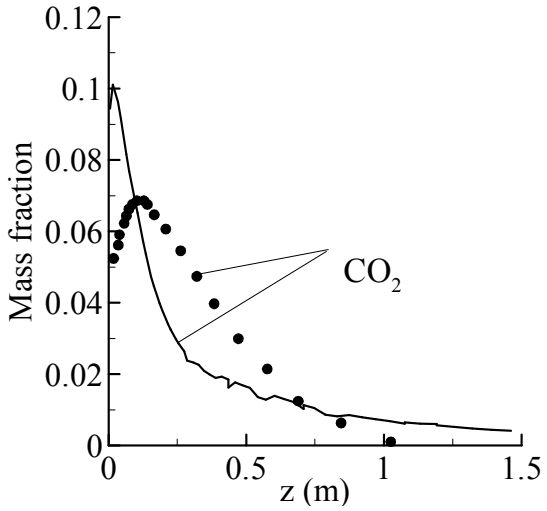

Figure 18. Comparison between the measured and predicted CO_2 concentration for HRR of 16 kW

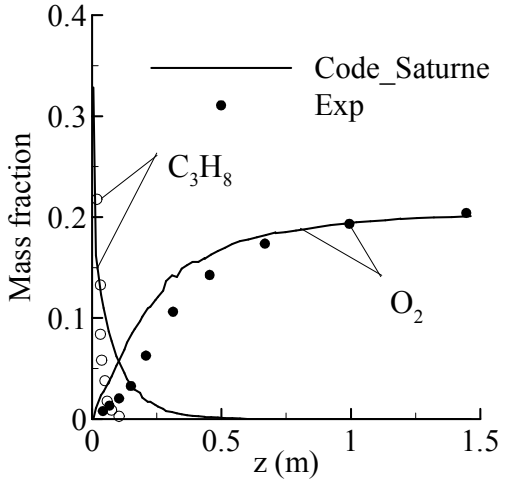

Figure 19. Comparison between the measured and predicted mean fuel and oxygen concentrations for HRR of 23 kW

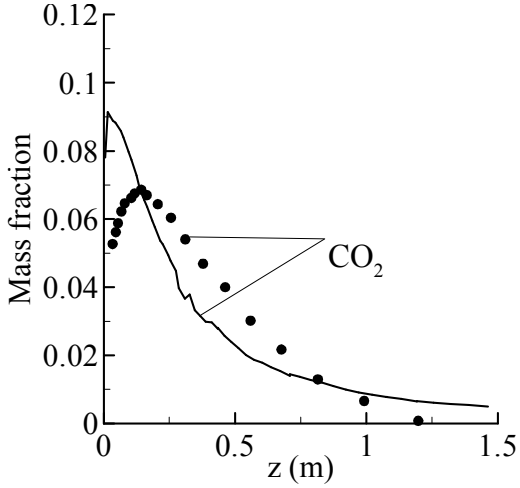

Figure 20. Comparison between the measured and predicted CO_2 concentration for HRR of 23 kW

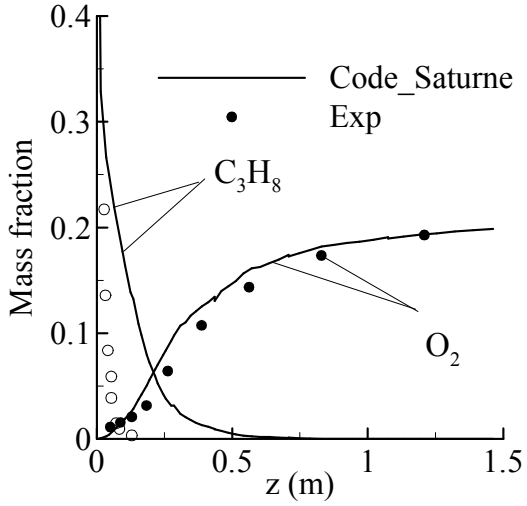

Figure 21. Comparison between the measured and predicted mean fuel and oxygen concentrations for HRR of 38 kW

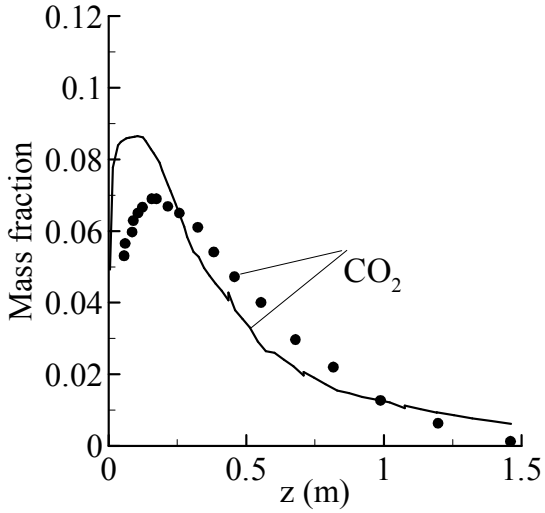

Figure 22. Comparison between the measured and predicted CO_2 concentration for HRR of 38 kW

One of the practical interests of pool-like fire simulation is the prediction of air entrainment from outside of the plume boundary. The entrainment rate is defined as the increase in the mean axial mass-flow rate of the gases with distance from the leading edge of the wall fire. As shown in Figs.23 and 24, the air entrainment is relatively low near the edge of the horizontal burner surface, due to very low upward gas velocities, w. Far away from the pool fire surface (z>0.5 m), buoyancy effects are important and the flow is strongly upward accelerated, entraining ambient air at larger mass flow rates. The predicted air entrainment rate for a HRR of 23 kW is compared in Figure 23 with a correlation [14] in which Quintiere gives a details description from buoyant pool fires.

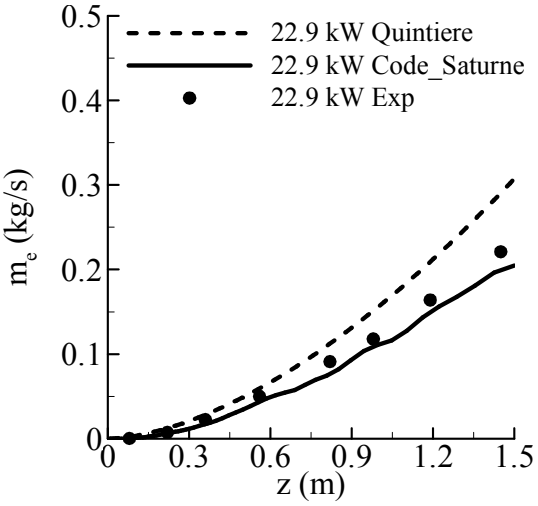

Figure 23. Comparison between the measured and predicted mean air entrainment for HRR of 23 kW

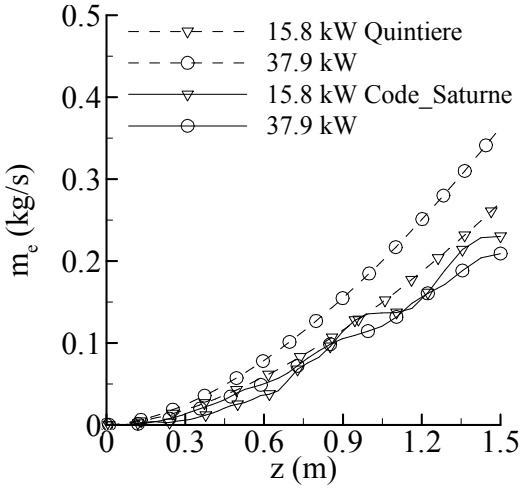

Figure 24. Air entrainment from the correlation and prediction for HRRs of 16 and 38 kW

The predicted air entrainment mass flow rates at distant downstream locations are in close agreement with the experimental values, indicating that the transverse velocity, u, is correctly predicted. As compared to the measurement, the entrainment is not well described by the correlation for the far downstream locations. Figure 24 shows a plot of the entrainment rate

versus the height for the heat release rates of 16 and 38 kW. Globally, the predicted entrainment rate closely follows the general entrainment behaviour of the correlation.

Determination of the time-averaged flame height is of particular concern due to the prediction of the convective/radiative heat fluxes, and as a consequence, of the flame propagation. The experimental flame height was determined through images processing and it was checked that the so-determined flame height corresponds to an average gas temperature of about 500°C [7]. This criterion is also used for determining the predicted flame height. From Figure 25, it can be seen that with increase of the heat release $\dot{Q}$, from 16, 23 to 38 kW, the predicted flame height increases sensitively from 0.2, 0.3 to 0.6 m. Different analytical relations [3,5,15] of the mean flame height are established. The predicted time-averaged flame height H_f, and the correlations as a function of the heat release rate are presented in Figure 25. The field model tends to underestimate the flame height by about 30% for the low heat release rate. It should be noted that the effects of external perturbations on the experimental data from which the correlations are established, become stronger for the low HRR. Globally, the effect of the heat release on the visible flame shape is consistent with a large body of correlations of Heskestad [15] and Delichatios [3]. Note that the distinction between the different regimes of the flame height is not obvious from the simulation data. It should be noted that the predicted flame shape seems rather sensitive to the definition for the visible flame shape (500 or 600°C) due to a significant stratification of the temperature.

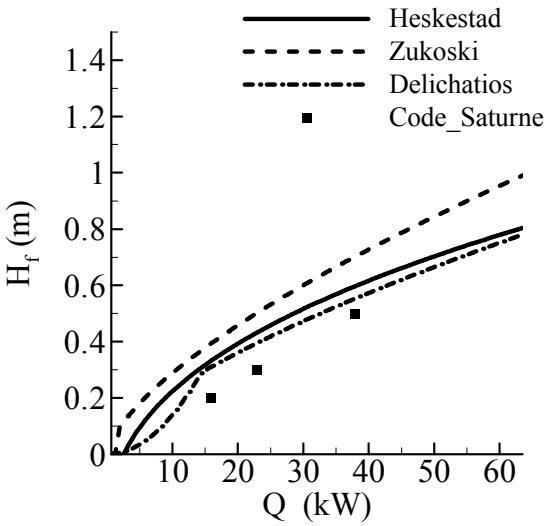

Figure 25. Comparison between the measured and predicted mean flame height as a function of the HRR

4. Conclusion

URANS successfully predicts the large fluctuation due to buoyancy instabilities permitted the description of some of the distinctive features of the turbulent free fires. These structures are thought to play a prominent part in the entrainment and mixing processes in fires. The numerical results show a good prediction of velocities, temperature and chemical species even with an infinitely fast one-step reaction model. According to the experiment, at the base of the fires, turbulence is not fully developed and the presence of large-scale buoyant instabilities produces a high flame extent. Ongoing work on finite one-step reaction and CO equilibrium should improve the prediction of the flame extent at the base of the fires for a better fire description.

References

[1] A. Bouhafid, J.P. Vantelon, P. Joulain and A.C. Fernandez-Pello, "On the flame structure at the base of a pool fire," Twenty-Second Symposium (International) on Combustion, Pittsburgh : The Combustion Institute, pp.1291-1298 (1988).

[2] Becker, H.A. and Yamazaki, S., "Entrainment, momentum flux and temperature in vertical free turbulent diffusion flames," Combustion and Flame, 33:123 (1978).

[3] M.A. Delichatios, "Air entrainment into buoyant jet and pool fires," *Combustion and Flame*, 70 :33–46, 1987.

[4] E. Gengembre, P. Cambray, D. Karmed, and J.C. Bellet, "Turbulent diffusion flames with large buoyancy effects," *Combustion science and technologies*, 41 :55–67, 1984.

[5] E.E. Zukoski, T. Kubota, and B. Cetegen, "Entrainment in fire plumes," *Fire Safety Journal*, 3 :107–121, 1981.

[6] E.J. Weckman and X.X. Sobiesak, "The oscillatory behaviour of medium scale pool fires, " *22th Symposium International on Combustion*, pages 1299–1310, 1988.

[7] M.O. Annarumma, J.M. Most, and P. Joulain, "On the numerical modeling of buoyancy-dominated turbulent vertical diffusion flames," *Combustion and flame*, 85 :403–415, 1991.

[8] EDF R&D. Code Saturne 1.3.2 theory and programmer's guide. Technical report.

[9] B.E. Launder and D.B. Spalding, "The numerical computation of turbulent flows," *Computational Methods in Applied Mechanics and Engineering*, 3 :269–289, 1974.

[10] A.T. Modak, "Radiation from products of combustion," *Fire Research*, 1 :339–361, 1979.

[11] J.B. Moss, C.D. Stewart, and K.J. Young, "Modeling soot formation and burnout in a high temperature laminar diffusin flame burning under oxygen-enriched conditions," *Combustion and flame*, 101 :491–500, 1995.

[12] J. Nagle and R.F. Strickland-Constable, "Oxidation of carbon between 1000 and 2000," *5th Carbon Conference*, 1 :154–164, 1962.

[13] K.B. McGrattan, H.R. Baum, and R.G. Rehm, "Large eddy simulations of smoke movement," *Fire Safety Journal*, 30 :161–178, 1998.

[14] J.G. Quintiere and B.S. Grove, "A unified analysis for fire plume," *27th Symposium International of Combustion*, pages 2757–2766, 1998.

[15]. G. Heskestad, "Engineering relations for fire plumes," *Fire Safety Journal*,5 :103–108, 1983.